CHAPTER-II

HYDROGEL ENCAPSULATED FLEXIBLE META-STRUCTURE ABSORBER

2.1 INTRODUCTION

Water exhibits high permittivity values in the microwave frequencies, with a loss tangent of ~0.5 [1]. The lossy characteristic of water has been used to develop absorbers by arranging water in arrays of periodic structures as mentioned in chapter I [1]. Water drops though placed over a rigid hydrophobic substrate, are only effective when placed horizontally, otherwise, may slide off from the surface due to gravitational pull. Evaporation of water can be another issue with these types of exposed absorbers when placed in open atmosphere or else it has to be placed inside rigid enclosures which are generally rigid and protruding [2-6]. Embedded water meta-atoms developed in [7] with the top completely sealed with hydrophobic cover can add more robustness to the water-based absorber. Here, tissue paper dipped in water is used to develop subwavelength resonating structure. Large-scale sample development with this technique is challenging and limits the shapes of the water resonators.

Hydrogels (water based gels) are three-dimensional (3D) networks of hydrophilic polymers that can hold a large quantity of water while retaining its structure due to physio-chemical cross-linking of individual polymer chains [8-11], Figure 2.1. The large water content in hydrogels has lossy properties close to that of water with advantage of facilitated handling during fabrication because of its semi-solid nature. Hydrogels are being increasingly used in flexible electronics for their flexibility, compressibility/stretchability and adhesiveness properties [11-15].

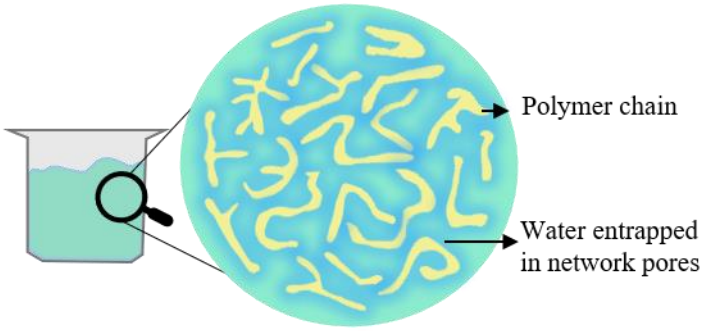

Figure 2.1 Schematic of hydrogel.

Absorbers, along with good absorption, are desired to absorb incident EM wave of any polarization. The incident EM wave with varying polarization angles, is basically given the same electromagnetic properties by structures that have rotational

symmetry in the plane of incidence. Thus, in structured absorbers like MMAs and MSAs, if the resonator geometry is having a good rotational symmetry, shows polarization immunity to the impinging EM wave [16-23]. Cuboids are well studied structures for designing resonators in MSAs [7, 24, 25] due to their simple geometry. With its four-fold symmetry it is possible to achieve a polarization insensitivity upto $\pm 90^{\circ}$. Here, hydrogel is considered for developing embedded subwavelength resonators to develop flexible MSAs shaped as cuboids.

The dimensions of the unit cell and the resonating structures are simulated and optimized using CST Microwave Suite simulation software using Trust Region Framework algorithm in Frequency Domain Solver based on finite element method (FEM), prior to fabrication. The fabricated MSAs are tested for absorption performance.

2.2 PREPARATION AND SELECTION OF FLEXIBLE HYDROGEL

Agar and PVA-borate based hydrogels are initially considered for development of resonating structures. These hydrogels contain ~90% of water which makes them lossy at microwave frequencies [26]. Moreover, they are readily available off-the-shelf and are easy to fabricate.

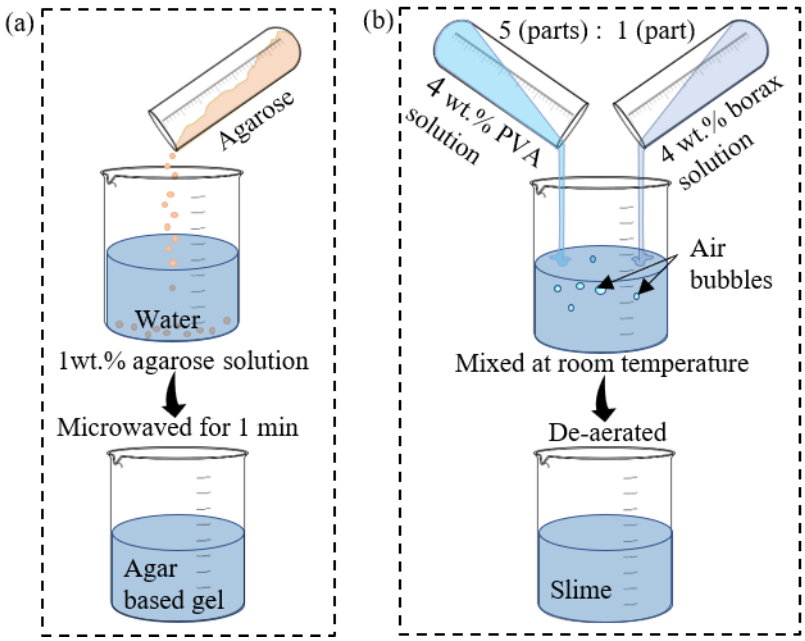

Figure 2.2 Preparation of (a) agar-based hydrogel and (b) slime.

Agar based hydrogel is prepared using 1 wt.% agarose low EEO (from SRL Pvt. Ltd.) in distilled water. The mixture is microwaved for ~ 1 min and allowed to settle for another 10 mins as shown in the schematic Figure 2.2(a). PVA-borate based hydrogel, commonly called slime, is developed by mixing 5 parts of 4 wt.% polyvinyl alcohol (PVA with M_w=1,46,000 g/mol) in distilled water solution and 1 part of 4 wt.% borax (Avantor Performance Materials India Ltd.) in distilled water through rigorous stirring as in [27]at room temperature, Figure 2.2(b). The gel is formed instantly.

The synthesized gels are tested for stretchability as well as for their self-healing ability. The gels are poured over petri dish. Both the gels are found to be sufficiently flexible, however on stretching slime shows better stretchability Fig. 2(a). Self-healing property is tested by slicing the gels into two parts and thereafter placing the edges closely in contact in Fig. 2(b). The sliced parts of slime join within 2 seconds, however, edges of agar-based gel remain separated as seen in Fig. 2(c).

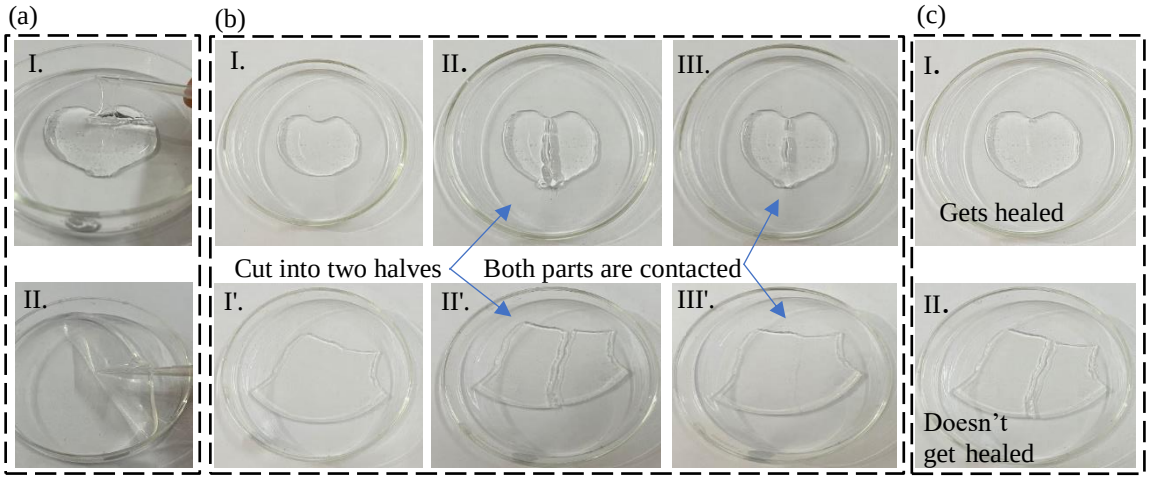

Figure 2.3 (a) Stretchability test of I. Slime and II. agar-based hydrogel. (b) I., II. & III. slime sliced and brought together and I'., II'. and III'. agar-based hydrogel sliced and edges brought together (c) I. Slime healed after 2 s II. agar-based gel does not heal.

Slime is chosen, here, as material for MSA's resonating structures.

2.2.1 Microwave characterization of slime

The values of complex permittivity of slime at room temperature is measured using a dielectric probe kit (Keysight N1501A) and analyzed using Agilent Vector Network Analyzer E8362C (VNA) in X-band [7]. First, the coaxial probe with open end is calibrated to reduce one port error. The calibration is done in three different loaded conditions: open circuit, short circuit and load (broadband). Figure 2.4 illustrates the

calibration process in three steps. In this instance, air serves as the open load, Figure 2.4(a), flexible conductive sheet as the short load, Figure 2.4(b) and water as broadband load, Figure 2.4(c), for the coaxial probe. The final permittivity values are obtained using the built-in, VNA-compatible Keysight N1500A materials measurement suite software.

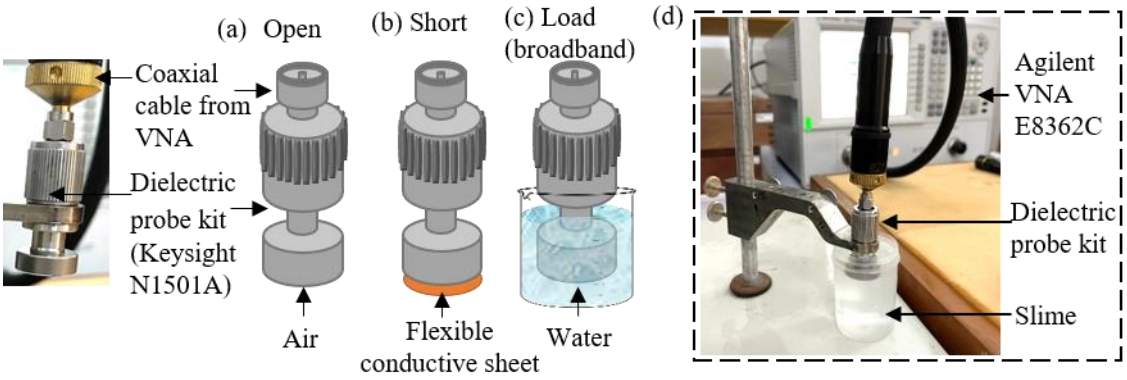

Figure 2.4 Calibration process of open-ended coaxial probe dielectric measurement setup in three stages – (a) open circuit with air, (b) short circuit with a flexible conductive sheet and (c) load (broadband) with water. (d) Complete setup alongwith slime.

Complex permittivity values of slime obtained at room temperature i.e., 25°C are plotted in Figure 2.5. A high loss of order of ~ 0.5 is observed for slime which is similar to that of water in the same frequency band [7]. In addition, slime is found to have density ~0.952 g cm^{-3} which is less than water, making it lighter.

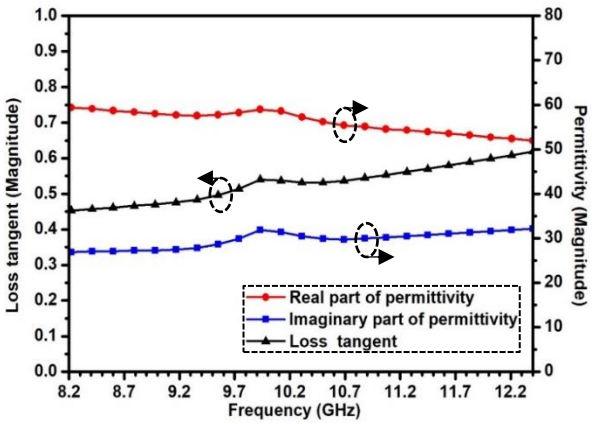

Figure 2.5 Complex permittivity values of slime at X-band.

2.3 SELECTION AND PREPARATION OF FLEXIBLE MATRIX

Polymers are low loss easy host materials to be used as matrix/substrate material for developing MSAs. Flexible polymers such a LLDPE, PET, rubber, [12-14] have

been reported to be used as substrate in flexible absorbers. As slime holds ~90% of water in its composition, hence a polymer impermeable to water is suitable. Silicone-rubber is one such polymers which has been reported for its hydrophobicity, good tensile strength and heat resistivity [7, 28, 29] and is chosen as matrix for embedding the slime resonators. Additionally, silicone-rubber is easily mouldable at room temperature ~25°C using hardener and is inert to external surrounding.

Silicone-rubber is prepared by mixing a room temperature vulcanizing viscous silicone (Make: Moldsil-India) of required amount with 5 wt.% curing agent as illustrated in Figure 2.6(a). The mixture is poured into additively manufactured, PLA (polylactic acid) moulds of desired shape and size and kept for about 12 hrs at room temperature (~28-30˚C) to cure as depicted in Figure 2.6(b).

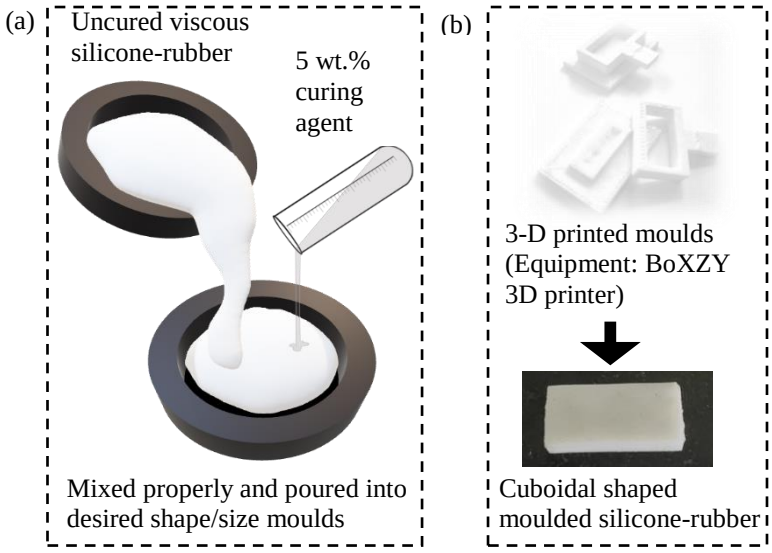

Figure 2.6 (a) Preparation of silicone-rubber. (b)Moulded silicone-rubber using 3D printed moulds.

2.3.1 Material characterization of silicone-rubber

The cured silicone-rubber is tested for its tensile strength, thermal stability and wettability. Tensile strength of silicone-rubber shows an elongation at break of ~600% as can be observed in Figure 2.7(a). TGA of silicone, Figure 2.7(b) shows 35% weight loss at ~ 350-500˚C and a sharp decomposition at 500˚C. The contact angle measurement of silicone with water is found to be $> 90^{\circ}$ confirming its hydrophobicity, Figure 2.7(c).

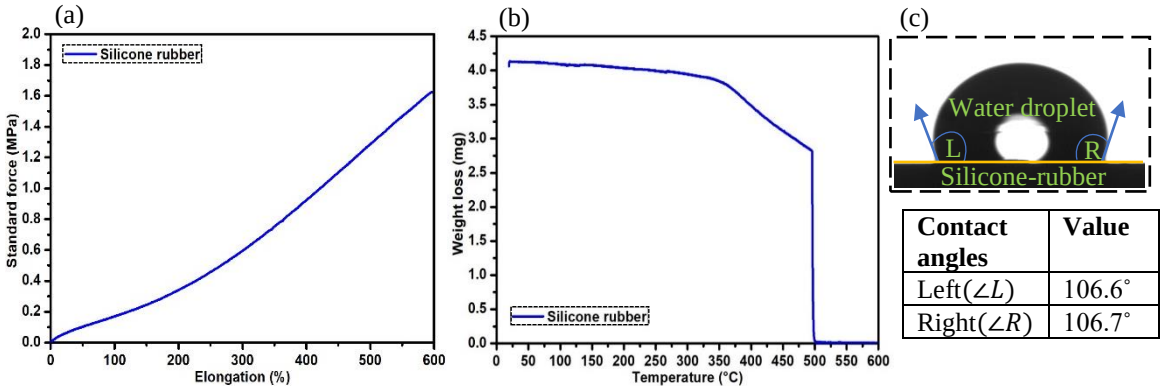

Contact angles	Value
Left($\angle L$)	106.6°
Right($\angle R$)	106.7°

Figure 2.7 (a) Tensile strength, (b) thermogravimetric analysis plot and (b) Wettability test of silicone-rubber.

Water absorption is measured after submerging silicone-rubber in water for a period of 72 hrs. due to its hydrophobicity, water absorbance is insignificantly low. All the observed values are placed in Table 2.1.

Table 2.1 Material parameters obtained for silicone-rubber.

Material parameter	Value	Equipment/method used
Density	1.1807 g cm^{-3}	Archimedes' principle
Elongation at break	600 % [**Figure 2.7(a)**]	5KN Electro mechanical Universal Testing Machine, Make: Zwick Roell, Model: Z005TN Proline
Decomposition temperature	> 300°C [**Figure 2.7(b)**]	Thermogravimetric analyzer (SHIMADZU-Model: TGA 50)
Wettability (Contact angles with water)	≥ 106° [**Figure 2.7(c)**]	Contact angle measurement system. (Data physics GmbH, Model: OCA 15 EC)
Water absorbance	~0.6%	Water absorption= $\frac{Weight_{submergered}-Weight_{actual}}{Weight_{actual}} \times 100$

2.3.2 Microwave characterization of silicone-rubber

Complex permittivity of silicone-rubber is characterized using an X-band waveguide kit (WR90-X11644A) compatible with Agilent Vector Network Analyzer E8362C (VNA). Two waveguide adapters as shown in Figure 2.8(a) are connected to each port of the dual port VNA and the setup is then calibrated employing transmission reflection line (TRL) technique [30, 31], Figure 2.8(b). A waveguide sized (22.86 mm × 10.16 mm) cuboidal shaped silicone-rubber sample of thickness ~3 mm is moulded as mentioned in the earlier section. The sample is placed inside the $\lambda/4$ waveguide slot spacer at the zero-reference plane of port 1 as shown in

Figure 2.8(c). Then power transmitted and reflected within the waveguide are measured and are represented by scattering parameters, also known as S-parameters. These parameters are defined as follows when port 1 is excited:

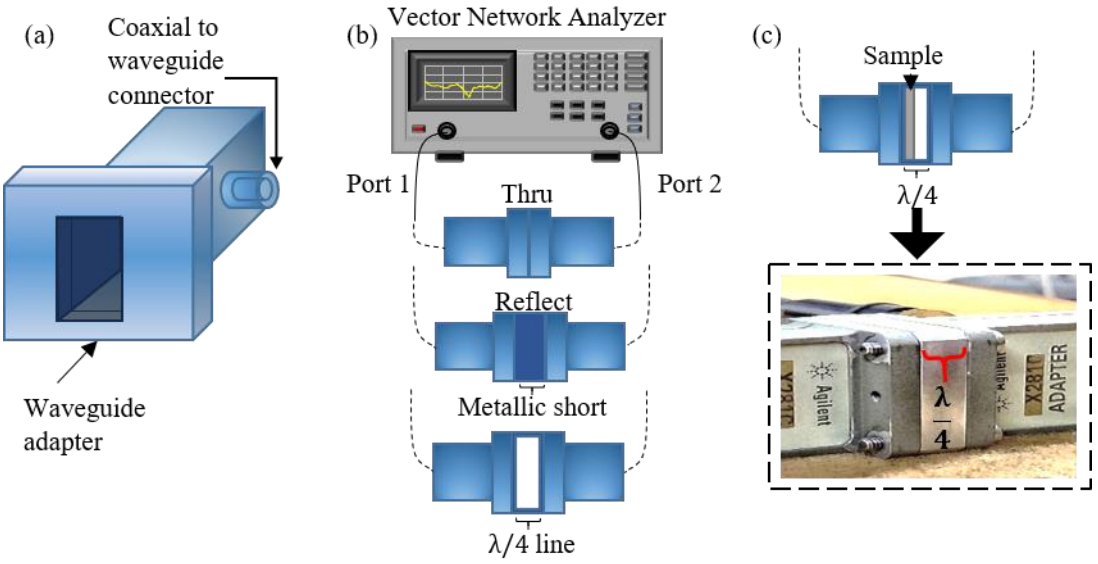

Figure 2.8 Schematic of (a) waveguide adapter and (b) TRL calibration process. (c) Image of waveguide setup.

$$S_{11} = \frac{Power\ reflected\ from\ port\ 1}{Power\ incident\ on\ port\ 1} \tag{2.1}$$

$$S_{21} = \frac{Power\ transmitted\ to\ port\ 2}{Power\ incident\ on\ port\ 1} \tag{2.2}$$

From these quantities, complex permittivity is computed using Nicolson-Ross-Weir technique using in-built Agilent 85071E material measurement software. The complex permittivity values of silicone-rubber are drawn in Figure 2.9 and is found to be $\sim 3.1 - j0.12$ which is almost constant throughout the X-band.

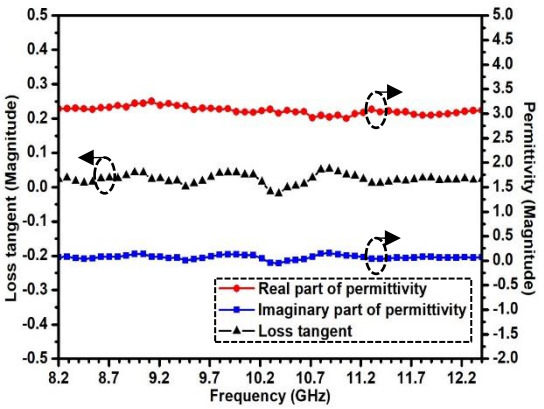

Figure 2.9 Complex permittivity of silicone-rubber.

2.4 MSA UNIT CELL DESIGN AND SIMULATION

Prior to the simulations, the measured complex permittivity values of both silicone-rubber and slime is imported to the software.

2.4.1 Slime-based MSA unit cell

The proposed MSA schematic is shown in Figure 2.10(a). The MSA unit cell is designed using regular symmetrical cuboidal structures as mentioned in section 2.1 to minimize both optimization and fabrication complexity. The MSA unit cell, Figure 2.10(b), consists of a single subwavelength-sized cuboidal shaped structure of slime enclosed in a silicone-rubber matrix backed by aluminium, Figures 2.10(b) and 2.10(c). Geometrical parameters are optimized in three steps- (1) to achieve absorption in the X-band, the height/thickness 'h' and 'w' of both the structures and the silicone-rubber layer below the slime cuboid 'g' are optimized. (2) Dimensions- 'l' and 'a' of the structures are optimized to obtain a widespread -10 dB bandwidth absorption over the band. (3) Thickness 't' of the top silicone layer is optimized to encompass the resonating structures completely with negligible effect on the absorption performance. Periodic boundary conditions are employed along x and y directions while EM wave is allowed to incident in the z-direction using a single Floquet port in the far-field of the unit cell to calculate the reflection coefficient as represented in Fig 2.10(d) to get the final design parameters presented in Table 2.2.

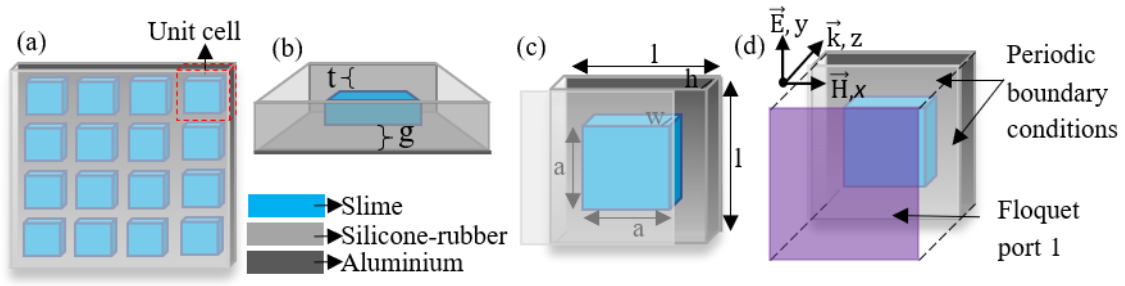

Figure 2.10 Schematic of (a) proposed slime based MSA, (b) unit cell of the MSA, (c) unit cell parameters and (d) simulation setup.

Table 2.2 Optimized unit cell parameters of slime based MSA.

Unit cell parameters	Description	Value (mm)
l	Length of the substrate	12.0
h	Height of the substrate	3.0
g	Thickness of layer below the slime cuboid	1.0
w	Height of the slime cuboid	1.0
a	Length of the slime cuboid	7.0
t	Thickness of layer above the slime cuboid	1
	Thickness of metal back (aluminium)	0.05

2.4.2 Simulated performance characteristics of slime-based MSA

It is imperative to maintain a minimum reflection at the air-absorber interface during the design process in order to maximise the incident electromagnetic wave inside the absorber, as was covered in section 1.2. The fundamental absorption expression in terms of S-parameters is calculated as

$$A_\omega = 1 - |S_{11}|^2 - |S_{21}|^2 \tag{2.3}$$

where, $|S_{11}|^2 = R_\omega$ and $|S_{21}|^2 = T_\omega$ are the reflectance and transmittance. A metal backed absorber has $T_\omega = 0$ reducing absorbance to

$$A_\omega = 1 - |S_{11}|^2 \tag{2.4}$$

Thus, reducing the reflectance term, $R_\omega = |S_{11}|^2$ alone will indicate enhanced absorption.

The normalized impedance at the air-absorber interface can be retrieved from S-parameters using equation [32] [4, 7, 33].

$$Z_a = Z_a{}' + Z_a{}'' = \sqrt{\frac{(1+S_{11})^2 - S_{21}^2}{(1-S_{11})^2 - S_{21}^2}} = \sqrt{\frac{(1+S_{11})^2}{(1-S_{11})^2}} = \pm\frac{1+S_{11}}{1-S_{11}} \tag{2.5}$$

Unity or maximum absorption is achieved when $Z' = 1$ and $Z'' = 0$.

The simulated reflection loss (co-polarization or at polarization angle (φ) of 0° and normal incidence i.e., incidence angle (θ) = 0°) values of the proposed absorber are plotted in Figure 2.11(a). The curves show a -36 dB reflection loss at the resonant frequency of 9.65 GHz and 2.01 GHz (-10 dB) bandwidth.

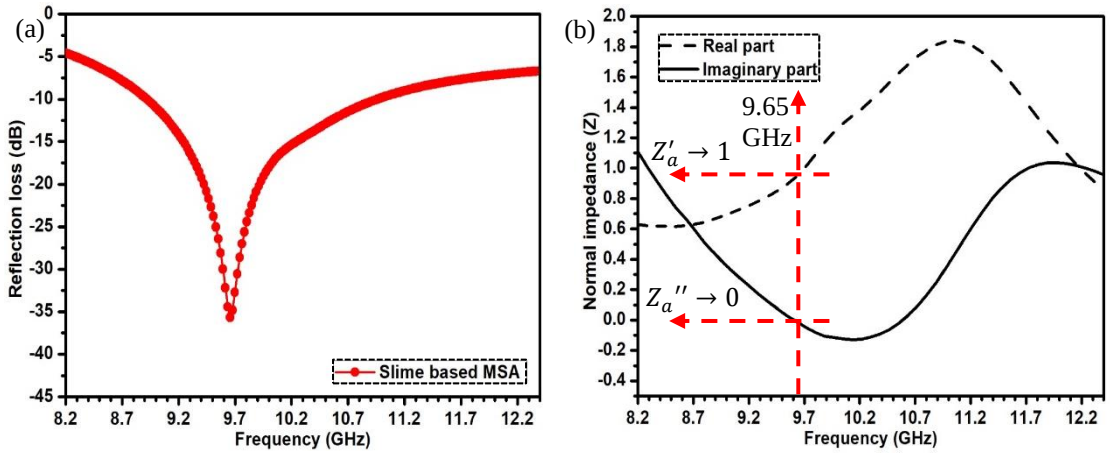

Figure 2.11 Simulated values of (a) reflection loss at normal incidence with polarization=0° and (b) normalized impedance of the slime based MSA in X-band.

The real $(Z_a')$and imaginary part (Z_a'') of the normalized impedance are plotted in Figure 2.11(b). At the resonating frequency, 9.65 GHz, $Z_a' \rightarrow 1$ and $Z_a'' \rightarrow 0$, Reflection loss characteristics for different polarization angles upto 90° (cross-polarization) are placed in Figure 2.12(a). The curves overlap and no variation is observed throughout the X-band range, thus indicating the absorber to be polarization independent. This could have resulted due to the four-fold symmetry of the designed structure. Figure 2.12(b) represents the absorption values of the slime MSA along with absorption observed in slime cuboid as well as silicone-rubber cuboid of the designed MSA size. The absorption in the MSA is a combined outcome of both dielectric loss in slime alongwith localised resonance in the structured slime resonators.

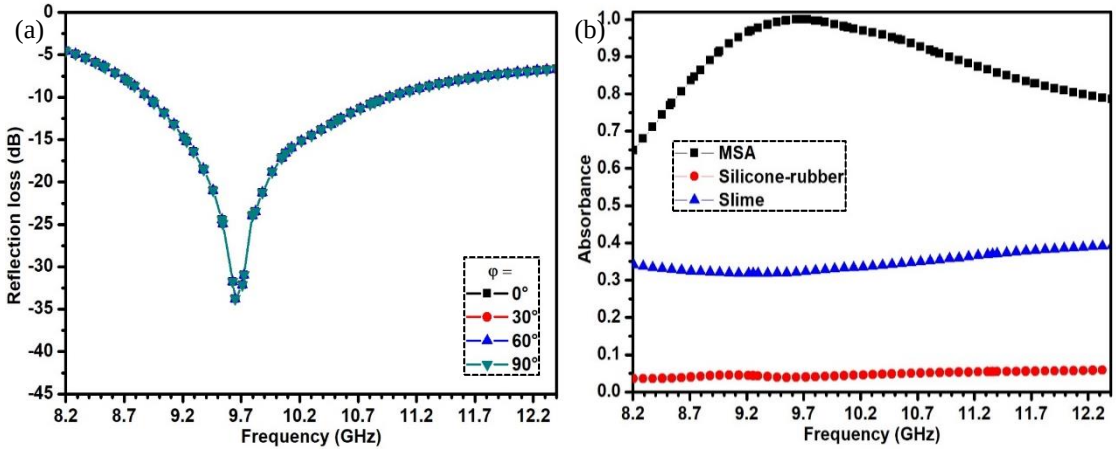

Figure 2.12 Simulated values of (a) reflection loss at different polarization angles and (b) absorption of the slime based MSA alongwith equal sized slime resonator and silicone-rubber in X-band.

The interaction of the designed MSA with microwave is comprehended by analysing the results of simulated field distribution at resonant frequency (9.65 GHz). Since the slime's permittivity value is higher than that of the silicone-rubber at X-band (Figure 2.13), the incident E-field is found to be concentrated towards the edges of the slime resonator, as shown in Figure 2.13(a). On the other hand, the H-field is localized in the centre of the slime resonators and the space between the ground and the resonator, Figure 2.13(b). As the alternating H-field enters the unit structure, two displacement current loops are generated inside the slime resonators, Figure 2.13(c). As can be seen in Figure 2.13 (d), the surface current on the ground plane flows counter to the loop current resulting in magnetic resonance that contributes to the effective permeability which greatly reduces the reflection loss at the resonant frequency. Both the induced E-field and the surface current at the metallic plate produce electric response that contributes to the effective permittivity. The field distributions closely resemble the absorption mechanism described in chapter I, section 1.3. Figure 2.13(e) shows the scattered power distribution in the MSA indicating the high dielectric loss of the hydrogel contributes to the microwave absorbance.

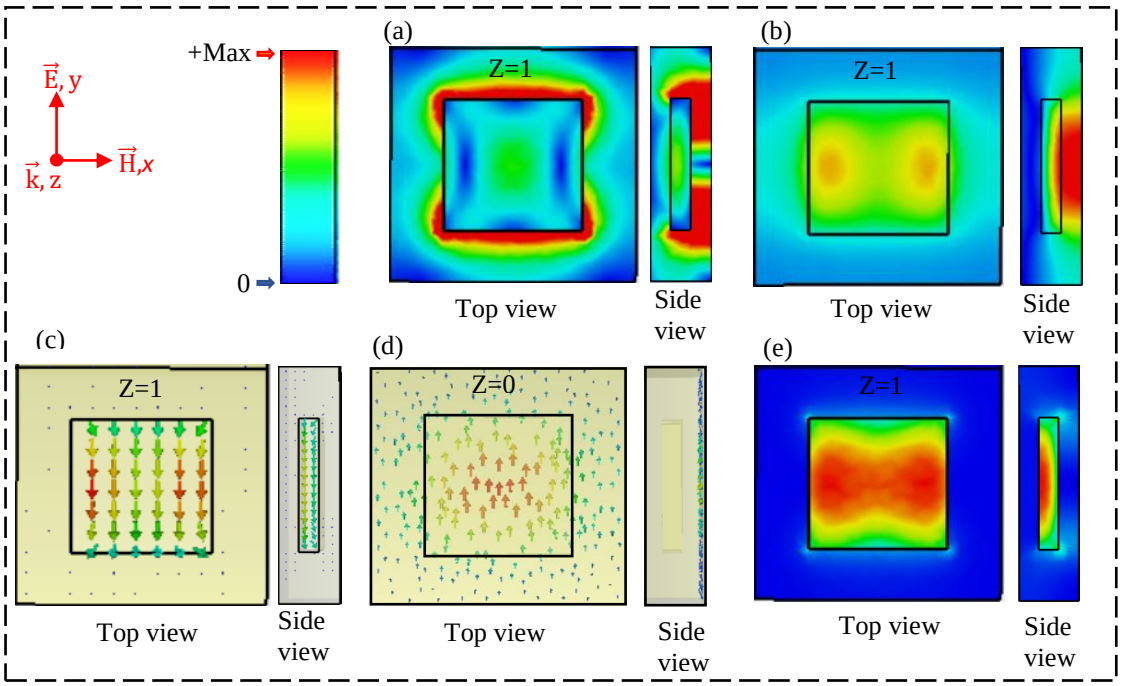

Figure 2.13 (a) E-field distribution, (b) H-field distribution, (c) induced current density, (d) surface current on the metallic ground plate and (e) scattered power distribution of slime based MSA at frequency 9.65 GHz.

2.5 FABRICATION AND MEASUREMENT

The absorber samples are fabricated using optimized dimensions from Table 2.2. Subsequently, the absorption performance of the developed absorber sample is measured.

2.5.1 Development of slime-based MSA

The in lab fabricated MSAs are sized to 22.86 × 10.16 mm^2 to fit in the waveguide kit used for absorption measurement discussed in next section. The fabrication is done broadly in three steps- firstly, PLA (Polylactic acid) moulds are additively manufactured using BoXZY 3D printer Figure 2.14(a) using which the silicone-rubber substrate is crafted. In the second step, the synthesized slime is poured inside the grooves as shown in Figure 2.14(b) and left undisturbed for ~2 h to settle and take shape. Lastly, the structure is cemented with a layer of silicone-rubber of thickness t= 1mm to further protect the slime from evaporation. The absorber is backed with aluminium tape of thickness ~0.05 mm. The developed absorber sample is shown in Figure 2.14(d).

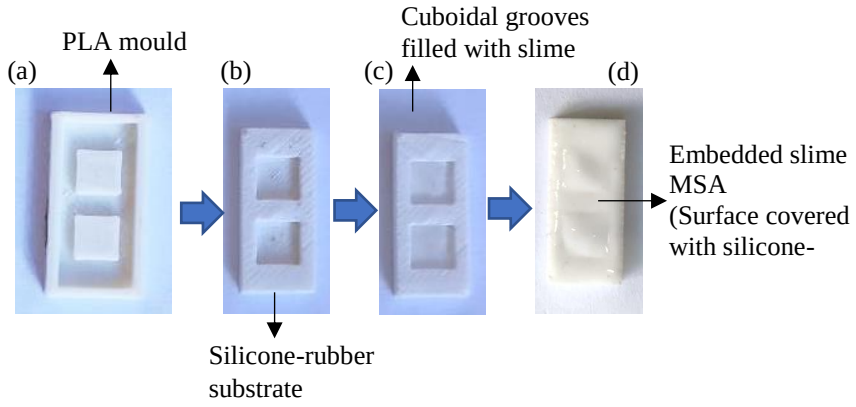

Figure 2.14 Fabrication of (a) PLA mould, (b) silicone-rubber substrate, (c) slime filled substrate, (d) complete slime based MSA.

2.5.2 Measurement of absorption performance of slime-based MSA

The developed absorber's absorption performance is measured using waveguide measurement technique. Figure 2.15 depicts a schematic of the method [7, 34-36] for a metal-backed absorber, or one with zero transmittance. The method is similar to the transmission-reflection method discussed in section 2.3.2 for measuring

microwave complex parameters; however, the technique differs in that a metal back is used to block signal transmission (figure 2.15 (a)). The sample is positioned at the λ/4 waveguide's short circuit end.

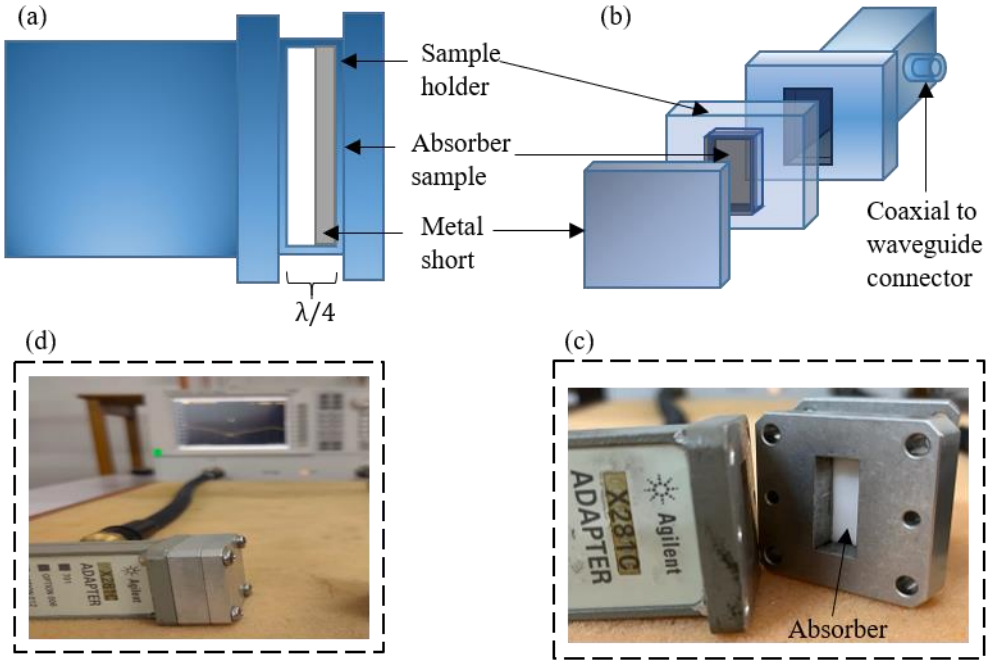

Figure 2.15 Waveguide measurement technique schematic (a) side view and (b) front view. Image of waveguide measurement technique (b) side view, (d) front view with sample mounted inside.

Plots of the experimental, as well as simulated reflection loss and absorbance, are presented in Figure 2.16. The experimental curve shows a reflection loss of −36.92 dB at 9.46 GHz with a -10 dB bandwidth of 2 GHz. The measured results are tabulated in Table 2.3 simultaneously with the simulated results. The minor variations observed in the results can be attributed to: (1) van der Waals forces within the slime molecules which are present in realistic slime material however there is no provision

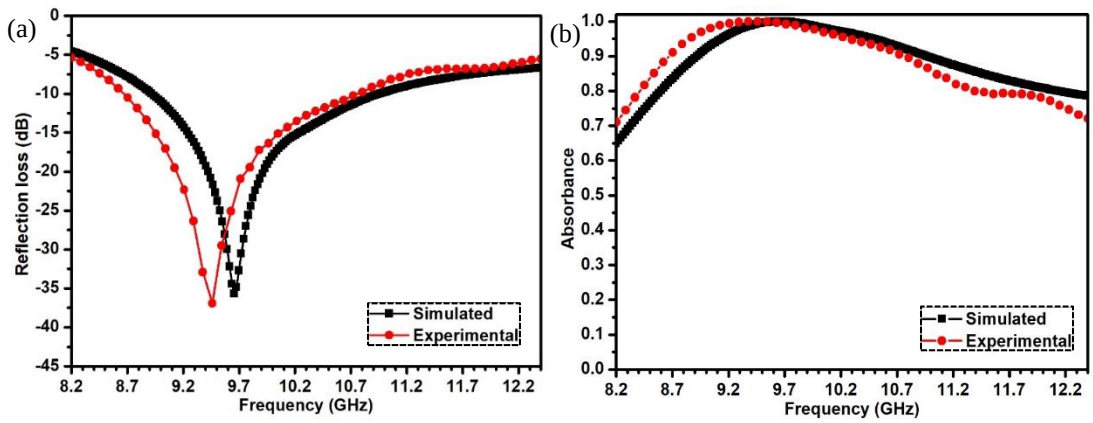

Figure 2.16 Measured (a) reflection loss and (b) absorbance spectra alongwith simulated results.

to take it into account in simulation. (2) additional filling of silicone-rubber in the MSA edges to fit the waveguide size. (3) Finite size of the sample is a constraint in the measurement technique which can induce some edge diffractions which otherwise is taken infinite in simulation.

Table 2.3 Absorption results of slime based MSA.

Absorber	**Resonant frequency (GHz)**	**Reflection loss (dB)**	**-10 dB Bandwidth (GHz)**	**>90% absorption (GHz)**	**% coverage of X-band**
Simulated	9.65	-36	2.01	8.9-10.91	47.8
Experimental	9.46	-36.92	2	8.7-10.7	47.6

2.6 CHAPTER SUMMARY

A flexible and planar slime based meta-structure absorber is developed embedding hydrogel (slime) resonating structures into flexible silicone-rubber matrix. The stretchable slime and highly flexible silicone-rubber have been advantageous in developing flexible absorber. The absorber is polarization independent due to structural symmetry and shows good absorption (>90%) at the resonant frequency, and flexibility with lightweight feature. The high dielectric loss tangent of slime assists broadband absorption in the X-band. The low water absorbance in the absorbers indicates that hydrophobic silicone-rubber successfully protects the filler material which also implies that MSAs are less affected from surrounding moisture. Additively manufactured mould minimizes the fabrication time making the absorber practically realizable. The non-toxic biocompatible nature of the material used can make it viable to be used in proximity to human. The detailed specifications of the developed slime based meta-structure absorber are tabulated in Table 2.4.

Table 2.4 Summary of slime based MSA's specifications.

Result→	*Measured*								*Simulated*
Parameter	**RF (GHz)**	**RL (dB)**	**% coverage of X-band**	**>90% A_ω (BW) (GHz)**	**Thickness**	**WA (%)**	**ρ (g cm^{-3})**	**P (mm)**	**PA-T**
Values	9.46	-36.92	47.6	8.7-10.7	3 mm ($0.082\lambda_0$)	0.6	~1.16	12	±90°
Note- RF- Resonant frequency, RL-reflection loss, A_ω-absorption, BW-bandwidth, λ_0-lowest operating frequency, WA-water absorbance, ρ- density, P-period, PA-T- polarization angle tolerance.									

REFERENCES

[1] Yoo, Y.J., et al., Metamaterial absorber for electromagnetic waves in periodic water droplets. *Scientific Reports*, 5(1): 14018, 2015.

[2] Ren, J. and J.Y. Yin, Cylindrical-water-resonator-based ultra-broadband microwave absorber. *Optical Materials Express*, 8(8): 2060-2071, 2018.

[3] Xie, J., et al., Water metamaterial for ultra-broadband and wide-angle absorption. *Optics express*, 26(4): 5052-5059, 2018.

[4] Zhang, X., et al., Broadband water-based metamaterial absorber with wide angle and thermal stability. *AIP Advances*, 10(5): 055211, 2020.

[5] Xie, J., et al., Truly all-dielectric ultrabroadband metamaterial absorber: Water-based and ground-free. *IEEE Antennas and Wireless Propagation Letters*, 18(3): 536-540, 2019.

[6] Du, L., et al., Ultra broadband microwave metamaterial absorber with multiple strong absorption peaks induced by sandwiched water resonators. *Applied Physics A*, 128(10): 864, 2022.

[7] Gogoi, D.J. and N.S. Bhattacharyya, Embedded dielectric water "atom" array for broadband microwave absorber based on Mie resonance. *Journal of Applied Physics*, 122(17): 175106, 2017.

[8] Ahmed, E.M., Hydrogel: Preparation, characterization, and applications: A review. *Journal of advanced research*, 6(2): 105-121, 2015.

[9] Bahram, M., N. Mohseni, and M. Moghtader. An introduction to hydrogels and some recent applications. *Emerging concepts in analysis and applications of hydrogels*, IntechOpen. 2016.

[10] Guo, Y., et al., Hydrogels and hydrogel-derived materials for energy and water sustainability. *Chemical Reviews*, 120(15): 7642-7707, 2020.

[11] Qin, T., et al., Recent progress in conductive self-healing hydrogels for flexible sensors. *Journal of Polymer Science*, 60(18): 2607-2634, 2022.

[12] Wang, H., et al., A highly elastic, Room-temperature repairable and recyclable conductive hydrogel for stretchable electronics. *Journal of Colloid and Interface Science*, 588: 295-304, 2021.

[13] Ying, B. and X. Liu, Skin-like hydrogel devices for wearable sensing, soft robotics and beyond. *Iscience*, 24(11), 2021.

[14] Chen, K., et al., Skin-Inspired Ultra-Tough Supramolecular Multifunctional Hydrogel Electronic Skin for Human–Machine Interaction*. Nano-Micro Letters*, 15(1): 102, 2023.

[15] Zhang, H., et al., A hydrogel-based electronic skin for touch detection using electrical impedance tomography*. Sensors*, 23(3): 1571, 2023.

[16] Zhu, L., et al., Polarization-independent and angle-insensitive electromagnetically induced transparent (EIT) metamaterial based on bi-air-hole dielectric resonators*. RSC advances*, 8(48): 27342-27348, 2018.

[17] Feng, J.-Q., et al., Polarization-independent and angle-insensitive metamaterial absorber using 90-degree-rotated split-ring resonators*. International Journal of Antennas and Propagation*, 2015: 6, 2015.

[18] Bağmancı, M., et al., Polarization independent broadband metamaterial absorber for microwave applications*. International Journal of RF and Microwave Computer-Aided Engineering*, 29(1): e21630, 2019.

[19] Ha, D.T., et al. Dual-Band, Polarization-Insensitive, Ultrathin and Flexible Metamaterial Absorber Based on High-Order Magnetic Resonance. In *Photonics*, 2021.8. 8. pages 574, 2021. MDPI.

[20] Hannan, S., et al., Wide bandwidth angle-and polarization-insensitive symmetric metamaterial absorber for X and Ku band applications*. Scientific Reports*, 10(1): 1-9, 2020.

[21] Hu, F., et al., Design of a polarization insensitive multiband terahertz metamaterial absorber*. Journal of Physics D: Applied Physics*, 46(19): 195103, 2013.

[22] Huang, X., et al., Triple-band polarization-insensitive wide-angle ultra-thin planar spiral metamaterial absorber*. Journal of Applied Physics*, 113(21): 213516, 2013.

[23] Kumari, N. and N. Gupta. Broadband polarization insensitive and angle independent metamaterial absorber. In *2017 Innovations in Power and Advanced Computing Technologies (i-PACT)*, 2017 pages 1-4, 2017. IEEE.

[24] Gogoi, D.J. and N.S. Bhattacharyya, Microwave metamaterial absorber based on aqueous electrolyte solution for X-band application*. Journal of Applied Physics*, 125(12): 125107, 2019.

[25] Huang, Y., et al., Ultrathin flexible carbon fiber reinforced hierarchical metastructure for broadband microwave absorption with nano lossy composite and multiscale optimization. *ACS applied materials interfaces,* 10(51): 44731-44740, 2018.

[26] Chen, X., et al., Hydrogel-based optically and mechanically manipulable broadband microwave absorber. *Nano Research*: 1-8, 2023.

[27] Casassa, E., A. Sarquis, and C. Van Dyke, The gelation of polyvinyl alcohol with borax: A novel class participation experiment involving the preparation and properties of a" slime". *Journal of Chemical Education*, 63(1): 57, 1986.

[28] Feng, L., S. Li, and S. Feng, Preparation and characterization of silicone-rubber with high modulus via tension spring-type crosslinking. *RSC advances*, 7(22): 13130-13137, 2017.

[29] Amin, M., M. Akbar, and S. Amin, Hydrophobicity of silicone-rubber used for outdoor insulation (an overview). *Rev. Adv. Mater. Sci*, 16(1-2): 10-26, 2007.

[30] Costa, F., et al., Electromagnetic characterisation of materials by using transmission/reflection (T/R) devices. *Electronics*, 6(4): 95, 2017.

[31] Rothwell, E.J., et al., Analysis of the nicolson-ross-weir method for characterizing the electromagnetic properties of engineered materials. *Progress In Electromagnetics Research*, 157: 31-47, 2016.

[32] Landy, N.I., et al., Perfect metamaterial absorber. *Physical review letters*, 100(20): 207402, 2008.

[33] Gogoi, D.J. and N.S. Bhattacharyya, Metasurface absorber based on water meta "molecule" for X-band microwave absorption. *Journal of Applied Physics*, 124(7): 075106, 2018.

[34] Borah, D. and N.S. Bhattacharyya. Design, fabrication and characterization of flexible and ultrathin microwave metamaterial absorber. In *2017 International Conference on Innovations in Electronics, Signal Processing and Communication (IESC)*, 2017 pages 190-193, 2017. IEEE.

[35] Kaur, K.P. and T. Upadhyaya, Dual-band perfect meta material absorber with polarization independence and wide incidence angle. 2018.

[36] Gordon, O., et al., Metamaterial absorbers realized in an X-band rectangular waveguide. *Chinese Physics B*, 21(11): 117801, 2012.